SICE Journal of Control, Measurement, and System Integration, Vol. 4, No. 1, pp. 001–009, January 2021

# Gaussian Process Based Visual Pursuit Control with Unknown Target Motion Learning in Three Dimensions

Marco OMAINSKA [*], Junya YAMAUCHI [*], Thomas BECKERS [**], Takeshi HATANAKA [***], Sandra HIRCHE [****], and Masayuki FUJITA [*,***]

**Abstract**: In this paper, we propose an observer-based visual pursuit control integrating 3-dimensional target motion learning by Gaussian Process Regression (*GPR*). We consider a situation where a visual sensor equipped rigid body pursuits a target rigid body whose velocity is unknown, but dependent on the target's pose. We estimate the pose from visual information and propose a Gaussian Process (*GP*) model to predict the target velocity from the pose estimate. We analyze stability of the proposed control by showing that estimation and control errors are ultimately bounded with high probability. Finally, simulations illustrate the performance of the proposed control schemes even if the visual measurement is corrupted by noise.

**Key Words:** vision-based estimation and control; rigid body motion; Gaussian Process; passivity

## 1. Introduction

Vision sensors are essential for the recognition of the external world because of their capability of obtaining rich information. The use of vision sensors in robot control has a long history [1] and their importance is increasing along with technological advances in mobile robots. Important applications for vision-equipped mobile robots include infrastructure inspections [2], bird control for farm [3] and biological studies [4]. This paper deals with the problem of estimating and tracking the motion of an object by a mobile robot equipped with a vision sensor.

Control methods that use a vision sensor to estimate the state of a robot in the environment and maintain it in a desired position have been proposed, for example in [5],[6]. The authors of [7],[8] consider tracking control of a target with simultaneous vision-based estimation of the unknown target pose in two dimensions. In contrast to [7] and [8], [9] proposes an observer-based control to pursuit a target rigid body moving in three dimensions. Furthermore, since the target motion is generally unknown, the approach in [9] extends the control law by a target body velocity generator model to achieve pursuit with zero steady-state error. However, since the information of the generator is required prior to the control system design, applicable situations are possibly limited. A promising technique to identify uncertain dynamics without the necessity of prior abundant knowledge is exploited in Machine Learning (*ML*).

Attention in the control community has been given to Gaussian Process (*GP*) models due to the strong Bayesian foundation including their advantage of estimating the uncertainty [10]. However, *ML* techniques typically suffer from lacking theoretical guarantees such as stability analysis, which limits the applicability to non-safety relevant systems. In [11]–[14], a *GP* model is utilized to learn the unknown dynamics and to analyze control performance and stability. By using the mean function of a *GP* model in a feed-forward manner, [13] aims to eliminate unmodeled dynamics and further provide a method to adjust the error feedback gains based on the *GP* variance. The author's recent publication [15] extends the result in [9] with the technique from [13] by integrating the learned *GP* target motion model into the visual pursuit control scheme to guarantee stability with high probability. In [15], a *GP* model learns the unknown body velocity as a function of the target's position for an observer-based control, assuming that the target is moving influenced by the environment, such as terrains and obstacles. However, since the target motion consists of both translation and rotation, the proposed visual pursuit control scheme is limited to a special class of target motions.

This paper proposes a stability-guaranteed visual pursuit control scheme based on a *GP* model that learns the unknown target body velocity, which is not only dependent on the position but also orientation. To begin with, we introduce rigid body motion, visual measurements and *GPR*. Then, the learning method by using *GP* models is addressed. Next, we propose a visual pursuit control law where the learned *GP* mean function is utilized to cancel the target body velocity, and the variance function to adjust error feedback gains. We then derive conditions on the gains to prove ultimate boundedness with high probability of the estimation and control errors. The main contributions of this paper are as follows: (i) extending the class of target body velocity to that of pose-dependent body velocity, (ii) proposing a visual pursuit control law based on the learned GP model and proving stability, (iii) showcase effect of gain adjustments by variance for noise attenuation in visual measurement.

In the following, Section 2 briefly describes the problem set-

[*] Department of Information Physics and Computing, The University of Tokyo, Tokyo, Japan
[**] Department of Electrical and Systems Engineering, University of Pennsylvania, Pennsylvania, USA
[***] Department of Systems and Control Engineering, Tokyo Institute of Technology, Tokyo, Japan
[****] Chair of Information-oriented Control (ITR), Department of Electrical and Computer Engineering, Technical University of Munich, Munich, Germany
E-mail: marcoomainska@g.ecc.u-tokyo.ac.jp
(Received xxx 01, 2020)
(Revised xxx 01, 2020)

 

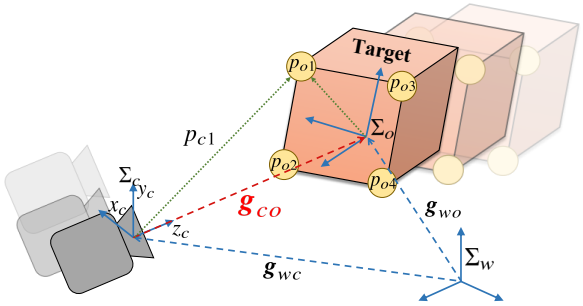


Fig. 1: Target rigid body and camera configuration.

ting and Section 3 addresses a method of *Visual Motion Observed*-based target motion learning. Thereafter, a new *visual pursuit control* with *GP*-prediction is proposed and stability is also analyzed in Section 4. Finally, simulations illustrate the efficiency of the proposed control law in Section 5.

## 2. Problem Setting

This section introduces the basics of *rigid body motion*, visual measurement [9], and the class of the target body velocity.

### 2.1 Rigid Body Motion

Assume a target and visual sensor moving in 3-dimensional space (Fig. 1) with inertial coordinate frame $\Sigma_w$ and body-fixed frames $\Sigma_o$, $\Sigma_c$. Their orientation and position are denoted by $e^{\hat{\xi}_{wi}\theta_{wi}} \in SO(3) := \left\{\boldsymbol{R} \in \mathbb{R}^{3\times3} \mid \boldsymbol{R}\boldsymbol{R}^\intercal = \boldsymbol{I}_3,\ \det(\boldsymbol{R}) = 1\right\}$, $i \in \{c, o\}$ and $\boldsymbol{p}_{wi} \in \mathbb{R}^3$, respectively. Further, $\boldsymbol{\xi}_{wi} \in \mathbb{R}^3$ describes the normalized rotation axis (i.e. $\boldsymbol{\xi}_{wi}^\intercal\boldsymbol{\xi}_{wi} = 1$) and $\theta_{wi} \in (-\pi, \pi]$ resembles the angle of rotation, while for simplicity hereon the shortened notation $\boldsymbol{\xi}\theta_{wi}$ is used. The operator $\wedge$ used in $e^{\hat{\xi}\theta_{wi}}$ maps a vector $\mathbb{R}^3$ to a $3\times3$ skew symmetric matrix, i.e. $\hat{\boldsymbol{a}}\boldsymbol{b} = \boldsymbol{a}\times\boldsymbol{b}$, $\boldsymbol{a}, \boldsymbol{b} \in \mathbb{R}^3$ where $\times$ the vector cross product [9]. On the contrary, $\vee$ denotes its inverse operator. The pair of both position and orientation is called the pose $\boldsymbol{g}_{wi} = \left(\boldsymbol{p}_{wi},\ e^{\hat{\xi}\theta_{wi}}\right) \in SE(3) := \mathbb{R}^3 \times SO(3)$ of $\Sigma_i$ with respect to $\Sigma_w$ for $i \in \{c, o\}$. To denote the pose $\boldsymbol{g}_{wi}$, we use the following matrix representation:

$$\boldsymbol{g}_{wo} = \begin{bmatrix} e^{\hat{\xi}\theta_{wo}} & \boldsymbol{p}_{wo} \\ 0 & 1 \end{bmatrix}, \quad \boldsymbol{g}_{wc} = \begin{bmatrix} e^{\hat{\xi}\theta_{wc}} & \boldsymbol{p}_{wc} \\ 0 & 1 \end{bmatrix}. \tag{1}$$

Similarly, the body velocity is defined as $\boldsymbol{V}_{wi}^b = \left(\boldsymbol{v}_{wi}^b,\ \boldsymbol{\omega}_{wi}^b\right) \in \mathbb{R}^6$ with the translational body velocity $\boldsymbol{v}_{wi}^b \in \mathbb{R}^3$ and the angular body velocity $\boldsymbol{\omega}_{wi}^b \in \mathbb{R}^3$. Then, the target motion and camera motion are described by

$$\begin{aligned} \dot{\boldsymbol{g}}_{wo} &= \boldsymbol{g}_{wo}\hat{\boldsymbol{V}}_{wo}^b, \qquad \hat{\boldsymbol{V}}_{wo}^b := \begin{bmatrix} \hat{\boldsymbol{\omega}}_{wo}^b & \boldsymbol{v}_{wo}^b \\ 0 & 0 \end{bmatrix}, \\ \dot{\boldsymbol{g}}_{wc} &= \boldsymbol{g}_{wc}\hat{\boldsymbol{V}}_{wc}^b, \qquad \hat{\boldsymbol{V}}_{wc}^b := \begin{bmatrix} \hat{\boldsymbol{\omega}}_{wc}^b & \boldsymbol{v}_{wc}^b \\ 0 & 0 \end{bmatrix}. \end{aligned} \tag{2}$$

Next, the relative pose of the target (2) relative to the camera (2) is defined as $\boldsymbol{g}_{co} := \boldsymbol{g}_{wc}^{-1}\boldsymbol{g}_{wo} \in SE(3)$ and by taking the derivative, one yields the *relative rigid body motion* (RRBM):

$$\dot{\boldsymbol{g}}_{co} = -\hat{\boldsymbol{V}}_{wc}^b\boldsymbol{g}_{co} + \boldsymbol{g}_{co}\hat{\boldsymbol{V}}_{wo}^b. \tag{3}$$

Here we assume that the camera is able to obtain its relative pose $\boldsymbol{g}_{wc}$. However, because the target pose $\boldsymbol{g}_{wo}$ is unknown as there is no way to communicate, $\boldsymbol{g}_{co}$ cannot be obtained either.

This paper considers a situation where the target rigid body is assumed to move under the influence of terrain and obstacles, and the body velocity can be considered as a map of the pose $\boldsymbol{g}_{wo}$ to $\mathbb{R}^6$, i.e. $\boldsymbol{V}_{wo}^b : SE(3) \to \mathbb{R}^6$. Note that this also means that each pose $\boldsymbol{g}_{wo} \in SE(3)$ is related to one single body velocity $\boldsymbol{V}_{wo}^b \in \mathbb{R}^6$. In order to learn the body velocity by *GPR* we need to define a proper vector representation, which is not a trivial problem since we also aim to guarantee system stability.

To this end, we define the ball with radius $\pi$ centered at the origin as $B_\pi(0) := \{\boldsymbol{a} \in \mathbb{R}^3 \mid \|\boldsymbol{a}\| \le \pi\}$. Since the exponential map is surjective from $B_\pi(0)$ to $SO(3)$ [16], all target orientation $e^{\hat{\xi}\theta_{wo}}$ are described by $\boldsymbol{\xi}\theta_{wo} \in B_\pi(0)$. Thus, we introduce the vector representation of $\boldsymbol{g} \in SE(3)$ as

$$\check{\boldsymbol{g}} := \begin{bmatrix} \boldsymbol{p} \\ \boldsymbol{\xi}\theta \end{bmatrix} \in \mathbb{R}^6 \tag{4}$$

and denote the body velocity as

$$\boldsymbol{V}_{wo}^b : \mathbb{R}^3 \times B_\pi(0) \to \mathbb{R}^6, \quad \check{\boldsymbol{g}}_{wo} \mapsto \boldsymbol{V}_{wo}^b\left(\check{\boldsymbol{g}}_{wo}\right). \tag{5}$$

This is a wider class of the body velocity than that assumed in [15] where the class of body velocity is assumed to be dependent just on the position $\boldsymbol{p}_{wo}$, namely, $\boldsymbol{V}_{wo}^b : \mathbb{R}^3 \to \mathbb{R}^6$. This paper uses a *GP* model to identify the unknown body velocity $\boldsymbol{V}_{wo}^b$ as a function of the pose $\check{\boldsymbol{g}}_{wo}$, and use it for visual pursuit control later in Section 4. The stability of the proposed visual pursuit system is also discussed there.

### 2.2 Visual Measurements

In line with [9,p.105] and following the author's results, the camera model of a pinhole camera is defined. It is used to measure feature points of the moving target in a 3D-environment as shown in Fig. 1. This process of extracting feature points in vast image data is common for real-time visual control scenarios [17]. Thus, we assume that the target has $n_f$ feature points whose position vectors relative to its object frame $\Sigma_o$ are denoted by $\boldsymbol{p}_{oi} \in \mathbb{R}^3$, $i = \{1, \cdots, n_f\}$, which are known a priori.

Let the position of $\boldsymbol{p}_{oi}$ as viewed from $\Sigma_c$ be $\boldsymbol{p}_{ci} = [x_{ci}\ y_{ci}\ z_{ci}]^\intercal \in \mathbb{R}^3$ satisfying $[\boldsymbol{p}_{ci}^\intercal\ 1]^\intercal = \boldsymbol{g}_{co}[\boldsymbol{p}_{oi}^\intercal\ 1]^\intercal$, $i = \{1, \cdots, n_f\}$. It is then projected onto the image plane of the camera by perspective projection [1] as a feature point $\boldsymbol{f}_i \in \mathbb{R}^2$:

$$\boldsymbol{f}_i = \frac{\lambda}{z_{ci}}\begin{bmatrix} x_{ci} \\ y_{ci} \end{bmatrix}, \tag{6}$$

with $\lambda > 0$ the focal length. By stacking (6) into a vector we obtain the *visual measurement* $\boldsymbol{f} := \begin{bmatrix} \boldsymbol{f}_1^\intercal & \cdots & \boldsymbol{f}_{n_f}^\intercal \end{bmatrix}^\intercal \in \mathbb{R}^{2n_f}$.

## 3. Observer-based Target Motion Learning

This section addresses how the target motion is learned. Consequently, the *GP* model for the purpose of target motion learning is defined, and in order to collect data for learning of the *GP* model, the *Visual Motion Observer* (*VMO*) [9] is introduced.

### 3.1 Gaussian Process Regression

Gaussian Process Regression (*GPR*) predicts unknown functions based on input output data and further provides a measure to quantify the model fidelity. Suppose one can measure data pairs of an unknown function $\boldsymbol{h} : \mathbb{R}^N \to \mathbb{R}^N$ as

$$\begin{aligned} &\boldsymbol{y} = \boldsymbol{h}(\boldsymbol{x}) + \boldsymbol{\epsilon} \in \mathbb{R}^N, \qquad \boldsymbol{x} \in \mathbb{R}^N \\ &\boldsymbol{\epsilon} \sim \mathcal{N}\left(0,\ \boldsymbol{\sigma}_n^2\right) \qquad \boldsymbol{\sigma}_n := \mathrm{diag}(\sigma_{n,1},\ \cdots,\ \sigma_{n,N}) \end{aligned} \tag{7}$$

with sub-Gaussian noise such that $|\epsilon_i| \le \sigma_{n,i}$ almost surely. The training dataset $\mathcal{D}$ consists of $M$ measurements of the input $\left\{\boldsymbol{x}^{\{m\}}\right\}_{m=1}^M$ and output $\left\{\boldsymbol{y}^{\{m\}}\right\}_{m=1}^M$ stacked into matrices

$$\mathcal{D} = \{\boldsymbol{X},\, \boldsymbol{Y}\}, \quad \begin{aligned} \boldsymbol{X} &\coloneqq \begin{bmatrix} \boldsymbol{x}^{\{1\}} & \cdots & \boldsymbol{x}^{\{M\}} \end{bmatrix} \in \mathbb{R}^{N\times M} \\ \boldsymbol{Y} &\coloneqq \begin{bmatrix} \boldsymbol{y}^{\{1\}} & \cdots & \boldsymbol{y}^{\{M\}} \end{bmatrix}^{\intercal} \in \mathbb{R}^{M\times N} \end{aligned} \tag{8}$$

Consequently, the prediction $\boldsymbol{y}^* \in \mathbb{R}^N$ at an input $\boldsymbol{x}^* \in \mathbb{R}^N$ is jointly Gaussian distributed with prior mean zero, and the mean and variance are defined as follows:

$$\begin{aligned} \boldsymbol{\mu}_i(\boldsymbol{y}_i^* \mid \mathcal{D},\, \boldsymbol{\varphi}_i,\, \boldsymbol{x}^*) &= \mathbf{K}_{\boldsymbol{\varphi}_i}(\boldsymbol{x}^*,\, \boldsymbol{X})\Big(\mathbf{K}_{\boldsymbol{\varphi}_i} + \sigma_{n,i}^2 \boldsymbol{I}_M\Big)^{-1} \boldsymbol{Y}_i \\ \boldsymbol{\Sigma}_i(\boldsymbol{y}_i^* \mid \mathcal{D},\, \boldsymbol{\varphi}_i,\, \boldsymbol{x}^*) &= \mathbf{K}_{\boldsymbol{\varphi}_i}(\boldsymbol{x}^*,\, \boldsymbol{x}^*) \\ &\quad - \mathbf{K}_{\boldsymbol{\varphi}_i}(\boldsymbol{x}^*,\, \boldsymbol{X})\Big(\mathbf{K}_{\boldsymbol{\varphi}_i} + \sigma_{n,i}^2 \boldsymbol{I}_M\Big)^{-1} \mathbf{K}_{\boldsymbol{\varphi}_i}(\boldsymbol{X},\, \boldsymbol{x}^*)\,. \end{aligned} \tag{9}$$

For notational convenience, the above terms are shortened to $\boldsymbol{\mu}_i(\boldsymbol{x}^*)$ and $\boldsymbol{\Sigma}_i(\boldsymbol{x}^*)$ hereon. Let the correlation between two inputs $(\boldsymbol{x},\, \boldsymbol{x}')$ be measured by the *SE-ARD kernel*

$$\mathbf{k}_{\boldsymbol{\varphi}_i}(\boldsymbol{x},\, \boldsymbol{x}') = \sigma_{f_i}^2 \exp\left(-\frac{1}{2}\sum_{j=1}^{N} \frac{\big(\boldsymbol{x}_j - \boldsymbol{x}_j'\big)^2}{l_{i,j}^2}\right). \tag{10}$$

**Remark 1** Since the SE-ARD kernel is an universal kernel, *GPR* with (10) can approximate any continuous function arbitrarily close on a compact set.

The entries of the *GP kernel matrix* $\mathbf{K}_{\boldsymbol{\varphi}_i} \coloneqq \mathbf{K}_{\boldsymbol{\varphi}_i}(\boldsymbol{X},\, \boldsymbol{X}) \in \mathbb{R}^{M\times M}$ represent the covariance between two elements of the dataset $\boldsymbol{X}$

$$\mathbf{K}_{\boldsymbol{\varphi}_i, j, j'} \coloneqq \mathbf{k}_{\boldsymbol{\varphi}_i}\big(\boldsymbol{X}_j,\, \boldsymbol{X}_{j'}\big), \quad j, j' \in \{1,\, \ldots,\, M\}\,.$$

$\mathbf{K}_{\boldsymbol{\varphi}_i}(\boldsymbol{x},\, \boldsymbol{X}) \in \mathbb{R}^M$ denotes the *vector-valued extended covariance function*. $\boldsymbol{Y}_i$, $\boldsymbol{X}_j$ resemble the $i$ th, $j$ th column of matrix $\boldsymbol{Y}$, $\boldsymbol{X}$ and $\boldsymbol{y}_i^*$, $\boldsymbol{x}_j^*$ is the $i$ th, $j$ th element of vector $\boldsymbol{y}^*$, $\boldsymbol{x}^*$. Lastly, $\boldsymbol{\varphi}_i \coloneqq \begin{bmatrix} l_{i,1}^2 & \cdots & l_{i,6}^2 & \sigma_{f_i}^2 \end{bmatrix} \in \mathbb{R}^7$ represents the set of *hyperparameters* with *lengthscales* $l_i^2 > 0$ and *signal variance* $\sigma_{f_i}^2 > 0$ which are typically obtained by likelihood maximization [10].

A kernel for $SE(3)$ is proposed in [18], and it can be expected to achieve better regression performance. However, we leave it as future work replacing (10) by the kernel proposed in [18].

### 3.2 Learning of Target Motion

The goal of this section is to propose a learning method for the unknown target body velocity $\boldsymbol{V}_{wo}^b(\check{\boldsymbol{g}}_{wo})$ by *GPR* using the target pose $\check{\boldsymbol{g}}_{wo}$ as the input $\boldsymbol{x}$, and the target body velocity $\boldsymbol{V}_{wo}^b$ as the output $\boldsymbol{y}$ in equation (7). In other words, the *GP* model in this paper predicts a function of the form

$$\boldsymbol{y} = \boldsymbol{V}_{wo}^b(\boldsymbol{x}) + \epsilon, \quad \boldsymbol{x} = \check{\boldsymbol{g}}_{wo} \tag{11}$$

Further, the following assumption is necessary such that target motion learning is feasible:

**Assumption 1** The target moves in a bounded 3-dimensional field, namely, its position belongs to a compact set $D \subset \mathbb{R}^3$.

Because target movements generally happen in bounded fields and environments, Assumption 1 is non-restrictive.

Since the Cartesian product of two compact sets is again a compact set, the following set is also compact from Assumption 1 and compactness of $B_\pi(0)$:

$$\mathcal{X} \coloneqq D \times B_\pi(0)\,. \tag{12}$$

The combined multi-variable Gaussian distribution in this paper is defined as the overall *GP* model

$$\begin{aligned} \boldsymbol{\mu}\big(\check{\boldsymbol{g}}_{wo}^*\big) &= [\boldsymbol{\mu}_1 \;\cdots\; \boldsymbol{\mu}_6]^{\intercal} \in \mathbb{R}^6 \\ \boldsymbol{\Sigma}\big(\check{\boldsymbol{g}}_{wo}^*\big) &= \mathrm{diag}(\boldsymbol{\Sigma}_1,\, \ldots,\, \boldsymbol{\Sigma}_6) \in \mathbb{R}^{6\times 6}\,. \end{aligned} \tag{13}$$

We now derive the following lemma regarding the upper bound of model fidelity from [19,Theorem 6]:

**Lemma 1** Consider the target model (2) and the trained GP model (13) with the dataset $\mathcal{D}$ (8). Further, define the *maximum information gain* after observing $M' = M + 1$ data pairs as

$$\zeta_i = \max_{\boldsymbol{X}'\in\mathcal{X}} \frac{1}{2}\log\Big|\boldsymbol{I}_{M'} + \sigma_{n,i}^{-2}\mathbf{K}_{\boldsymbol{\varphi}_i}'\Big|,\; i \in \{1, \ldots, 6\} \tag{14}$$

with the dataset $\boldsymbol{X}' \coloneqq \begin{bmatrix} \boldsymbol{x}^{\{1\}} & \cdots & \boldsymbol{x}^{\{M'\}} \end{bmatrix} \in \mathbb{R}^{6\times M'}$ and $\mathbf{K}_{\boldsymbol{\varphi}_i}' \coloneqq \mathbf{K}_{\boldsymbol{\varphi}_i}(\boldsymbol{X}',\, \boldsymbol{X}') \in \mathbb{R}^{M'\times M'}$. Then, the model error is bounded by

$$\mathcal{P}\Big\{\forall \check{\boldsymbol{g}}_{wo} \in \mathcal{X},\; \Big\|\boldsymbol{\mu}\big(\check{\boldsymbol{g}}_{wo}\big) - \boldsymbol{V}_{wo}^b\big(\check{\boldsymbol{g}}_{wo}\big)\Big\| \le \Big\|\beta^{\intercal}(\delta)\boldsymbol{\Sigma}^{\frac{1}{2}}\big(\check{\boldsymbol{g}}_{wo}\big)\Big\|\Big\} \ge \delta \tag{15}$$

for any probability $\delta \in (0,\, 1)$ and elements of $\beta \in \mathbb{R}^6$ satisfy

$$\beta_i(\delta) = \sqrt{2\big\|\boldsymbol{V}_{wo_i}^b\big\|_{\mathbf{k}_{\boldsymbol{\varphi}_i}}^2 + 300\,\zeta_i \ln^3\left(\frac{M+1}{1-\sqrt[6]{\delta}}\right)} \tag{16}$$

where $\big\|\boldsymbol{V}_{wo_i}^b\big\|_{\mathbf{k}_{\boldsymbol{\varphi}_i}}$ is the bounded reproducing kernel Hilbert space norm associated with kernel $\mathbf{k}_{\boldsymbol{\varphi}_i}$ of $i$ th element of $\boldsymbol{V}_{wo}^b$.

Note that one can find an upper-bound $\bar{\Delta}$ of the model error as

$$\Big\|\beta^{\intercal}(\delta)\boldsymbol{\Sigma}^{\frac{1}{2}}\big(\check{\boldsymbol{g}}_{wo}\big)\Big\| \le \bar{\Delta}(\delta) \tag{17}$$

on $\mathcal{X}$ [20]. Furthermore, the parameter $\beta_i$ increases with the amount of data, but due to a sub-linear dependency of $\zeta_i$ on the number of data observed, the bound in (15) can be decreased [12]. Even though $\boldsymbol{V}_{wo_i}^b$ is not an element of the *RKHS* associated with $\mathbf{k}_{\boldsymbol{\varphi}_i}$ (i.e., $\big\|\boldsymbol{V}_{wo_i}^b\big\|_{\mathbf{k}_{\boldsymbol{\varphi}_i}}$ is not bounded), Remark 1 assures their boundedness for functions arbitrarily close to $\boldsymbol{V}_{wo_i}^b$ [20].

### 3.3 Visual Motion Observer

Prior to control phase, let the *VMO* estimate the relative pose $\boldsymbol{g}_{co}$ of a moving target (2) in the perspective of a camera (2) in a training phase in order to collect data of the target pose $\bar{\boldsymbol{g}}_{wo} \coloneqq \boldsymbol{g}_{wc}\bar{\boldsymbol{g}}_{co}$. The estimated target velocity can be calculated from $\bar{\boldsymbol{V}}_{wo}^b = \bar{\boldsymbol{g}}_{wo}^{-1}\dot{\bar{\boldsymbol{g}}}_{wo}$ and $\dot{\bar{\boldsymbol{g}}}_{wo} = \dot{\boldsymbol{g}}_{wc}\bar{\boldsymbol{g}}_{co} + \boldsymbol{g}_{wc}\dot{\bar{\boldsymbol{g}}}$.

The estimate of $\boldsymbol{g}_{co}$ is denoted by $\bar{\boldsymbol{g}}_{co} = \Big(\bar{\boldsymbol{p}}_{co},\, e^{\hat{\bar{\boldsymbol{\xi}}}\bar{\boldsymbol{\theta}}_{co}}\Big)$ and the model for motion estimation [9,Section 6] is given by

$$\dot{\bar{\boldsymbol{g}}}_{co} = -\hat{\boldsymbol{V}}_{wc}^b\bar{\boldsymbol{g}}_{co} - \bar{\boldsymbol{g}}_{co}\hat{\boldsymbol{u}}_e\,. \tag{18}$$

The goal of this section is to find an observer input $\boldsymbol{u}_e$ for training phase, and later in Section 4 for control phase.

The vector representation of $\boldsymbol{g}$ [1] is given as

$$vec(\boldsymbol{g}) \coloneqq \begin{bmatrix} \boldsymbol{p} \\ \mathrm{sk}\Big(e^{\hat{\boldsymbol{\xi}}\boldsymbol{\theta}}\Big)^{\vee} \end{bmatrix} \in \mathbb{R}^6 \tag{19}$$

with $\mathrm{sk}(\boldsymbol{A}) \coloneqq (1/2)(\boldsymbol{A} - \boldsymbol{A}^{\intercal})$, $\boldsymbol{A} \in \mathbb{R}^{3\times 3}$. Then, the estimation error $\boldsymbol{g}_{ee} = \Big(\boldsymbol{p}_{ee},\, e^{\hat{\boldsymbol{\xi}}\boldsymbol{\theta}_{ee}}\Big) \in SE(3)$ and its vector representation $\boldsymbol{e}_e \in \mathbb{R}^6$ are defined as

[1] Using $vec(\boldsymbol{g})$ is crucial to show passivity of the visual pursuit system in Lemma 2, but disadvantageous for *GP* learning and prediction since $\mathrm{sk}\Big(e^{\hat{\boldsymbol{\xi}}\boldsymbol{\theta}}\Big)^{\vee} = \boldsymbol{\xi}\sin\boldsymbol{\theta} = \boldsymbol{\xi}\sin(\boldsymbol{\theta} + \pi/2)$ for $|\boldsymbol{\theta}| \in [0,\, \pi/2]$ [9]. Hence, there might be conflicts in the rotation data.

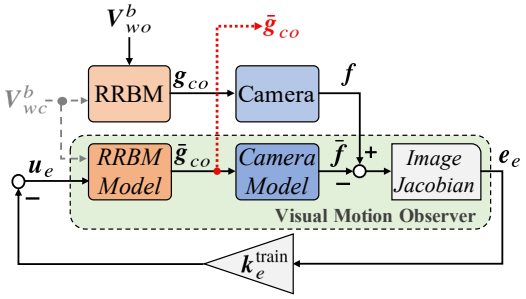


Fig. 2: Block diagram of the *VMO* for collecting data.

$$\boldsymbol{g}_{ee} \coloneqq \bar{\boldsymbol{g}}_{co}^{-1}\boldsymbol{g}_{co}, \quad \boldsymbol{e}_e \coloneqq vec(\boldsymbol{g}_{ee}). \tag{20}$$

Consider the following assumption for motion estimation:

**Assumption 2** The estimation error angle is bounded by $|\boldsymbol{\theta}_{ee}(t)| \leq \pi/2,\ \forall t \geq 0$.

Because of $\boldsymbol{g}_{co}$ being unavailable, $\boldsymbol{g}_{ee}$ and $\boldsymbol{e}_e$ cannot be computed along definition (20). However, the estimated visual measurement $\bar{\boldsymbol{f}}$ can be calculated from $\bar{\boldsymbol{g}}_{co}$ and (6), thus the error $\boldsymbol{f}_e \coloneqq \boldsymbol{f} - \bar{\boldsymbol{f}}$ can be obtained. Further, for small $|\boldsymbol{\theta}_{ee}|$ (Assumption 2), it holds that $\boldsymbol{f}_e = J(\bar{\boldsymbol{g}}_{co})\boldsymbol{e}_e$, with the *image Jacobian* $J(\bar{\boldsymbol{g}}_{co})$ from [9,p.108]. Since the pseudo-inverse $J^\dagger(\bar{\boldsymbol{g}}_{co})$ of $J(\bar{\boldsymbol{g}}_{co})$ can be obtained when $n_f \geq 4$, the estimation error can be calculated from

$$\boldsymbol{e}_e = J^\dagger(\bar{\boldsymbol{g}}_{co})\boldsymbol{f}_e\,. \tag{21}$$

In order to design observer input $\boldsymbol{u}_e$, one derives the estimation error (20) from the definitions of *RRBM* (3) and *VMO* (18) as

$$\dot{\boldsymbol{g}}_{ee} = \hat{\boldsymbol{u}}_e\boldsymbol{g}_{ee} + \boldsymbol{g}_{ee}\hat{\boldsymbol{V}}^b_{wo}. \tag{22}$$

Defining the notation $\boldsymbol{V}^b_{ee} \coloneqq \left(\boldsymbol{g}_{ee}^{-1}\dot{\boldsymbol{g}}_{ee}\right)^\vee$ yields $\boldsymbol{V}^b_{ee} = \mathrm{Ad}_{(\boldsymbol{g}_{ee}^{-1})}\boldsymbol{u}_e + \boldsymbol{V}^b_{wo}\left(\breve{\boldsymbol{g}}_{wo}\right)$ with the *adjoint transformation* of $\boldsymbol{g}$ [9] given as

$$\mathrm{Ad}_{(\boldsymbol{g})} \coloneqq \begin{bmatrix} e^{\hat{\boldsymbol{\xi}}\boldsymbol{\theta}} & \hat{\boldsymbol{p}}e^{\hat{\boldsymbol{\xi}}\boldsymbol{\theta}} \\ 0 & e^{\hat{\boldsymbol{\xi}}\boldsymbol{\theta}} \end{bmatrix} \in \mathbb{R}^{6\times 6}. \tag{23}$$

In addition, we define $\mathrm{Ad}_{\left(e^{\hat{\boldsymbol{\xi}}\boldsymbol{\theta}}\right)} \coloneqq \mathrm{Ad}_{\left(0,\, e^{\hat{\boldsymbol{\xi}}\boldsymbol{\theta}}\right)}$. Finally, the observer input $\boldsymbol{u}_e = -k_e^{\text{train}}\boldsymbol{e}_e$ with $k_e^{\text{train}} > 0$ makes the equilibrium $\boldsymbol{e}_e = 0$ asymptotically stable when the target is static ($\boldsymbol{V}^b_{wo} \equiv 0$) [9, Corollary 6.3]. Furthermore, with the result of $L_2$ stability in [9, Theorem 6.4], one can still get good performance for a moving target when the gain $k_e^{\text{train}}$ is large enough. Therefore, a high gain assures that one can train a *GP* model from the estimated pose assuming that $\breve{\boldsymbol{g}}_{wo} \approx \breve{\boldsymbol{g}}_{wo}$. The block diagram of the *VMO* for target motion learning is shown in Fig. 2.

## 4. Visual Pursuit Control with GP Target Motion

The goal is now to combine the *VMO* with the *GP* model in feed-forward fashion from the previous Section 3 for a *visual pursuit control* scenario. In contrast to the author's previous publication [15], the full pose is incorporated for the control scheme. Further, differently to Section 3, it is not assumed that $\breve{\boldsymbol{g}}_{wo} \approx \breve{\boldsymbol{g}}_{wo}$ since it is too risky in a control setting to use large gains that might amplify noise severely.

### 4.1 GP-enhanced Visual Pursuit Control

The *visual pursuit control* (*VPC*) aims to drive the relative pose $\boldsymbol{g}_{co}$ from (3) to a desired pose $\boldsymbol{g}_d \in SE(3)$ utilizing the *VMO* from Section 3.3. Similar to the estimation error (20), one defines the pose control error $\boldsymbol{g}_{ce} = \left(\boldsymbol{p}_{ce},\, e^{\hat{\boldsymbol{\xi}}\boldsymbol{\theta}_{ce}}\right) \in SE(3)$ and control error $\boldsymbol{e}_c \in \mathbb{R}^6$ as

$$\boldsymbol{g}_{ce} \coloneqq \boldsymbol{g}_d^{-1}\bar{\boldsymbol{g}}_{co}, \quad \boldsymbol{e}_c \coloneqq vec(\boldsymbol{g}_{ce})\,. \tag{24}$$

We assume the following for the control error:

**Assumption 3** The control error angle is bounded by $|\boldsymbol{\theta}_{ce}(t)| \leq \pi/2,\ \forall t \geq 0$.

This assumption is in general satisfied due to the given scenario as the target moves slower than the robot with camera.

Again, differentiating the control error (24) we achieve

$$\begin{aligned} \dot{\boldsymbol{g}}_{ce} &= \hat{\boldsymbol{u}}_c\boldsymbol{g}_{ce} - \boldsymbol{g}_{ce}\hat{\boldsymbol{u}}_e\,, \\ \boldsymbol{u}_c &\coloneqq -\mathrm{Ad}_{(\boldsymbol{g}_d^{-1})}\boldsymbol{V}^b_{wc}\,, \quad \hat{\boldsymbol{u}}_c = -\boldsymbol{g}_d^{-1}\hat{\boldsymbol{V}}^b_{wc}\boldsymbol{g}_d \end{aligned} \tag{25}$$

and thus the *control error system* results to

$$\boldsymbol{V}^b_{ce} \coloneqq \left(\boldsymbol{g}_{ce}^{-1}\dot{\boldsymbol{g}}_{ce}\right)^\vee = -\boldsymbol{u}_e + \mathrm{Ad}_{(\boldsymbol{g}_{ce}^{-1})}\boldsymbol{u}_c \tag{26}$$

with $\boldsymbol{V}^b_{ce}$ the control error velocity. Finally, the combination of both $\boldsymbol{V}^b_{ce}$ and $\boldsymbol{V}^b_{ee}$ obtained in Section 3.3 yields the *error system*

$$\begin{aligned} \begin{bmatrix} \boldsymbol{V}^b_{ce} \\ \boldsymbol{V}^b_{ee} \end{bmatrix} &= \begin{bmatrix} \mathrm{Ad}_{(\boldsymbol{g}_{ce}^{-1})} & -\boldsymbol{I}_3 \\ 0 & \mathrm{Ad}_{(\boldsymbol{g}_{ee}^{-1})} \end{bmatrix}\boldsymbol{u} + \begin{bmatrix} 0 \\ \boldsymbol{I}_6 \end{bmatrix}\boldsymbol{V}^b_{wo}\left(\breve{\boldsymbol{g}}_{wo}\right) \\ \boldsymbol{u} &\coloneqq \begin{bmatrix} \boldsymbol{u}_c \\ \boldsymbol{u}_e \end{bmatrix} \in \mathbb{R}^{12}\,. \end{aligned} \tag{27}$$

The goal is now to find a suitable input $\boldsymbol{u}$ that adapts the *GP* model from Section 3.2.

To this end, we first show passivity of the error system. We define the positive definite function

$$\begin{aligned} S &\coloneqq \frac{1}{2}\left\|\boldsymbol{p}_{ce}\right\|^2 + \phi\left(e^{\hat{\boldsymbol{\xi}}\boldsymbol{\theta}_{ce}}\right) + \frac{1}{2}\left\|\boldsymbol{p}_{ee}\right\|^2 + \phi\left(e^{\hat{\boldsymbol{\xi}}\boldsymbol{\theta}_{ee}}\right) \\ \phi\left(e^{\hat{\boldsymbol{\xi}}\boldsymbol{\theta}}\right) &\coloneqq \frac{1}{2}\mathrm{tr}\left(\boldsymbol{I}_3 - e^{\hat{\boldsymbol{\xi}}\boldsymbol{\theta}}\right) \end{aligned} \tag{28}$$

and the total error $\boldsymbol{e} = [\boldsymbol{e}_c^\intercal\ \boldsymbol{e}_e^\intercal]^\intercal \in \mathbb{R}^6$ and output $\boldsymbol{\nu} \in \mathbb{R}^{12}$ as

$$\boldsymbol{\nu} \coloneqq \boldsymbol{N}\boldsymbol{e}\,, \quad \boldsymbol{N} \coloneqq \begin{bmatrix} \boldsymbol{I}_6 & 0 \\ -\mathrm{Ad}_{\left(e^{-\hat{\boldsymbol{\xi}}\boldsymbol{\theta}_{ce}}\right)} & \boldsymbol{I}_6 \end{bmatrix}. \tag{29}$$

Then, the following lemma is derived:

**Lemma 2 (Lemma 7.1 [9])** The time derivative of $S$ (28) along with the *error system* (27) obeys

$$\dot{S} = \boldsymbol{\nu}^\intercal\boldsymbol{u} + \boldsymbol{e}^\intercal\begin{bmatrix} 0 \\ \mathrm{Ad}_{\left(e^{\hat{\boldsymbol{\xi}}\boldsymbol{\theta}_{ee}}\right)} \end{bmatrix}\boldsymbol{V}^b_{wo}\left(\breve{\boldsymbol{g}}_{wo}\right). \tag{30}$$

**Proof:** Refer to [9,Equation (6.2)]. ■

Hence, for the case of the static target ($\boldsymbol{V}^b_{wo} \equiv 0$), the *error system* (27) is passive from input $\boldsymbol{u}$ to output $\boldsymbol{\nu}$ with respect to the storage function $S$. Thus, for the given scenario of a moving target ($\boldsymbol{V}^b_{wo} \neq 0$) under Assumption 2, we propose the following input $\boldsymbol{u}$ using $\bar{\boldsymbol{g}}_{wo} = \boldsymbol{g}_{wc}\boldsymbol{g}_{co}$ as:

$$\boldsymbol{u} = -\boldsymbol{K}\left(\boldsymbol{\Sigma}\left(\breve{\bar{\boldsymbol{g}}}_{wo}\right)\right)\boldsymbol{\nu} - \underbrace{\begin{bmatrix} \mathrm{Ad}_{\left(e^{\hat{\boldsymbol{\xi}}\boldsymbol{\theta}_{ce}}\right)}\mathrm{Ad}_{\left(e^{\hat{\boldsymbol{\xi}}\boldsymbol{\theta}_{ee}}\right)} \\ \mathrm{Ad}_{\left(e^{\hat{\boldsymbol{\xi}}\boldsymbol{\theta}_{ee}}\right)} \end{bmatrix}}_{:=\widetilde{\mathrm{Ad}}}\boldsymbol{\mu}\left(\breve{\bar{\boldsymbol{g}}}_{wo}\right). \tag{31}$$

The first term achieves asymptotic stability of the equilibrium point $\boldsymbol{e} = 0$ when $\boldsymbol{V}^b_{wo} = 0$ [9,Corollary 7.2]. In addition, the

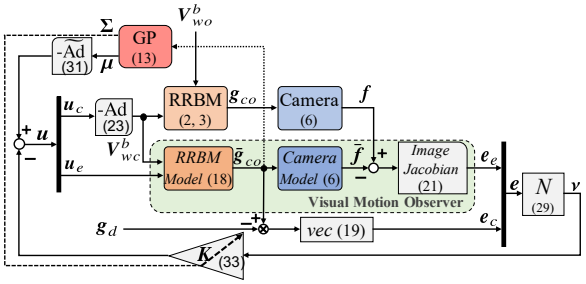


Fig. 3: Block diagram of *VPC* with designed input (31).

mean $\boldsymbol{\mu}\left(\breve{\boldsymbol{g}}_{wo}\right)$ from (13) attempts to cancel the disturbance $\boldsymbol{V}_{wo}^{b}$ in feed-forward fashion. Moreover, the error feedback gain $\boldsymbol{K}$ varies depending on the GP model confidence $\boldsymbol{\Sigma}\left(\breve{\boldsymbol{g}}_{wo}\right)$, which is designed later. Hereafter, we denote $\boldsymbol{\Sigma}\left(\breve{\boldsymbol{g}}_{wo}\right)$ as simply $\boldsymbol{\Sigma}$. The rotational error $e^{\hat{\boldsymbol{\xi}}\boldsymbol{\theta}_{ee}}$ in $\mathrm{Ad}_{\left(e^{\hat{\boldsymbol{\xi}}\boldsymbol{\theta}_{ee}}\right)}$ can be calculated from $\mathrm{sk}\left(e^{\hat{\boldsymbol{\xi}}\boldsymbol{\theta}_{ee}}\right)^{\vee}$ under Assumption 2 from [21] as follows:

$$e^{\hat{\boldsymbol{\xi}}\boldsymbol{\theta}_{ee}} = \exp\left(\frac{\sin^{-1}\left(\left\|\mathrm{sk}\left(e^{\hat{\boldsymbol{\xi}}\boldsymbol{\theta}_{ee}}\right)^{\vee}\right\|\right)}{\left\|\mathrm{sk}\left(e^{\hat{\boldsymbol{\xi}}\boldsymbol{\theta}_{ee}}\right)^{\vee}\right\|}\mathrm{sk}\left(e^{\hat{\boldsymbol{\xi}}\boldsymbol{\theta}_{ee}}\right)\right). \tag{32}$$

As a remark, the controller is similar to [15], but rather than using only the estimate target position as an input for the *GP* model, both estimates of position and orientation are used in this approach, since a wider class of the target velocity is considered as given by (5). Furthermore, let the controller $\boldsymbol{K}\left(\boldsymbol{\Sigma}\left(\breve{\boldsymbol{g}}_{wo}\right)\right)$ be of the form

$$\begin{aligned}
&\boldsymbol{K}(\boldsymbol{\Sigma}) \coloneqq \mathrm{diag}(\boldsymbol{K}_c(\boldsymbol{\Sigma}),\, \boldsymbol{K}_e(\boldsymbol{\Sigma})) \in \mathbb{R}^{12\times 12}\\
&\boldsymbol{K}_c(\boldsymbol{\Sigma}) \coloneqq \mathrm{diag}(k_{c_1}(\boldsymbol{\Sigma}),\, \cdots,\, k_{c_6}(\boldsymbol{\Sigma})) \in \mathbb{R}^{6\times 6}\\
&\boldsymbol{K}_e(\boldsymbol{\Sigma}) \coloneqq \mathrm{diag}\left(k_{e_p}(\boldsymbol{\Sigma})\boldsymbol{I}_3,\, k_{e_R}(\boldsymbol{\Sigma})\boldsymbol{I}_3\right) \in \mathbb{R}^{6\times 6}\\
&0 < \underline{k}_{c_i} \le k_{c_i}(\boldsymbol{\Sigma}) \le \bar{k}_{c_i}, \quad i \in \{1,\ldots,6\}\\
&0 < \underline{k}_{e_p} \le k_{e_p}(\boldsymbol{\Sigma}) \le \bar{k}_{c}\,, \quad 0 < \underline{k}_{e_R} \le k_{e_R}(\boldsymbol{\Sigma}) \le \bar{k}_{e_R}\,.
\end{aligned} \tag{33}$$

where $k_{c_i}(\boldsymbol{\Sigma})$, $k_{e_p}(\boldsymbol{\Sigma})$, $k_{e_R}(\boldsymbol{\Sigma})$ are designed to be continuous in $\boldsymbol{\Sigma}$. Furthermore, remember that $\boldsymbol{\mu}$ is dependent on the estimate $\breve{\boldsymbol{g}}_{wo}$ rather than on the real $\breve{\boldsymbol{g}}_{wo}$ which is unavailable. However, the difference between $\boldsymbol{\mu}\left(\breve{\boldsymbol{g}}_{wo}\right)$ and $\boldsymbol{\mu}\left(\breve{\breve{\boldsymbol{g}}}_{wo}\right)$ can be bounded based on Lipschitz continuity of the *GP* mean function and its kernel $\mathbf{k}_{\boldsymbol{\varphi}_i}$ [10]:

**Lemma 3** The error between the prediction of $\boldsymbol{V}_{wo}^{b}(\breve{\boldsymbol{g}}_{wo})$ by the real $\breve{\boldsymbol{g}}_{wo}$ and the estimate $\breve{\breve{\boldsymbol{g}}}_{wo}$ on $\mathcal{X}$ is bounded as follow:

$$\left\|\boldsymbol{\mu}\left(\breve{\boldsymbol{g}}_{wo}\right) - \boldsymbol{\mu}\left(\breve{\breve{\boldsymbol{g}}}_{wo}\right)\right\| \le L_p\left\|\boldsymbol{p}_{ee}\right\| + 2\pi L_\theta\,, \tag{34}$$

where $L_p$, $L_\theta$ denote Lipschitz constants.

**Proof:** Refer to Appendix A. ■

Lemma 3 is necessary for stability analysis of the error system shown in Fig. 3.

### 4.2 Stability Analysis

This section addresses the main theorem on stability of the system in Fig. 3 based on the notion of ultimate boundedness. Now we show the main result.

**Theorem 1** Consider the error system (27) with input (31) and a trained *GP* model (13) with dataset $\mathcal{D}$ (8). Further, suppose that Assumptions 1 to 3 hold and the gain $\boldsymbol{K}\left(\boldsymbol{\Sigma}\left(\breve{\boldsymbol{g}}_{wo}\right)\right)$ in (33) satisfies the following for all $\breve{\boldsymbol{g}}_{wo}$:

$$\boldsymbol{Q}(\boldsymbol{\Sigma}) \coloneqq \begin{bmatrix} \boldsymbol{K}_c(\boldsymbol{\Sigma}) + \boldsymbol{K}_e(\boldsymbol{\Sigma}) & -\boldsymbol{K}_e(\boldsymbol{\Sigma}) \\ -\boldsymbol{K}_e(\boldsymbol{\Sigma}) & \boldsymbol{K}_e(\boldsymbol{\Sigma}) - \Gamma \end{bmatrix} > 0 \tag{35}$$

where the matrix $\Gamma$ is defined as

$$\Gamma \coloneqq \frac{1}{2}\left(\frac{1}{\gamma_1^2} + \frac{L_p}{\gamma_2^2} + \frac{L_\theta}{\gamma_3^2}\right)\boldsymbol{I}_6 + \frac{L_p\gamma_2^2}{2}\begin{bmatrix} \boldsymbol{I}_3 & 0 \\ 0 & 0 \end{bmatrix} \tag{36}$$

with positive constants $\gamma_1,\, \gamma_2,\, \gamma_3 > 0$ and $L_p$, $L_\theta$ obtained in Lemma 3. Then, there exist a $\rho(\delta) > 0$ and a $T(\delta) \ge 0$ with any probability $\delta \in (0,1)$ such that

$$\mathcal{P}\{\|\boldsymbol{e}(t)\| \le b,\ \forall t \ge T\} \ge \delta \tag{37}$$

$$b(\delta) \coloneqq \sqrt{\frac{\gamma_1^2\bar{\Delta}^2(\delta) + 4\gamma_3^2\pi L_\theta}{2\eta\lambda_Q}}, \quad \eta \in (0,1) \tag{38}$$

for any $\boldsymbol{e}(0)$ satisfying $\|\boldsymbol{e}(0)\| \le \rho(\delta)$ where the minimum eigenvalue of $\boldsymbol{Q}(\boldsymbol{\Sigma})$ is represented by $\lambda_{\min}(\boldsymbol{Q}(\boldsymbol{\Sigma}))$, and $\lambda_{\boldsymbol{Q}} \coloneqq \min_{\boldsymbol{\Sigma}} \lambda_{\min}(\boldsymbol{Q}(\boldsymbol{\Sigma}))$.

**Proof:** Refer to Appendix B. ■

Inferring from the gain condition (35), large Lipschitz constants $L_p$ and $L_\theta$ imply large control and observer gains. This may indicate that the unknown function $\boldsymbol{V}_{wo}^{b}$ may change sensitively with small variations in $\breve{\boldsymbol{g}}_{wo}$.

Note that [15,Theorem 1] only assures a probabilistic bounded error for the *GP*-enhanced *VPC* for a class of target body velocities $\boldsymbol{V}_{wo}^{b}(\boldsymbol{p}_{wo})$, and thus $\Gamma$ and the ball (37) lack terms specific to the orientation. Furthermore, due to the matrix $\boldsymbol{Q}$ being a function of the variance $\boldsymbol{\Sigma}\left(\breve{\boldsymbol{g}}_{wo}\right)$, the condition (35) has to be confirmed for all $\breve{\boldsymbol{g}}_{wo}$, which makes the design difficult. Hence, we derive the following corollary for a simpler gain condition with the simplified control gain

$$\begin{aligned}
&\boldsymbol{K}_c(\boldsymbol{\Sigma}) \coloneqq \mathrm{diag}\left(k_{c_p}(\boldsymbol{\Sigma})I_3,\, k_{c_R}(\boldsymbol{\Sigma})I_3\right) \in \mathbb{R}^{6\times 6}\\
&0 < \underline{k}_{c_p} \le k_{c_p}(\boldsymbol{\Sigma}) \le \bar{k}_{c_p}, \quad 0 < \underline{k}_{c_R} \le k_{c_R}(\boldsymbol{\Sigma}) \le \bar{k}_{c_R}.
\end{aligned} \tag{39}$$

**Corollary 1** Consider the error system (27) with input (31) and a trained *GP* model (13) with dataset $\mathcal{D}$ (8). Further, suppose that Assumptions 1 to 3 hold and $\underline{k}_{c_i}, \underline{k}_{e_i}$ satisfy

$$\frac{2\underline{k}_{c_i}\underline{k}_{e_i}}{\underline{k}_{c_i} + \underline{k}_{e_i}} > \frac{1}{\gamma_1^2} + \left(\frac{1}{\gamma_2^2} + \alpha_i\gamma_2^2\right)L_p + \frac{L_\theta}{\gamma_3^2}, \quad i \in \{p,\, R\} \tag{40}$$

with $\gamma_1, \gamma_2, \gamma_3 > 0$ and $\alpha_p = 1$, $\alpha_R = 0$. Then, there exist a $\rho(\delta) > 0$ and a $T(\delta) \ge 0$ with any probability $\delta \in (0,1)$ such that (37) with (38) holds for any $\boldsymbol{e}(0)$ satisfying $\|\boldsymbol{e}(0)\| \le \rho(\delta)$.

**Proof:** From the *Schur complement*, the condition (35) is simplified to $\boldsymbol{K}_e(\boldsymbol{\Sigma}) - \Gamma - \boldsymbol{K}_e(\boldsymbol{\Sigma})(\boldsymbol{K}_c(\boldsymbol{\Sigma}) + \boldsymbol{K}_e(\boldsymbol{\Sigma}))^{-1}\boldsymbol{K}_e(\boldsymbol{\Sigma}) > 0$. Due to a difference in $\Gamma$, it follows two conditions on the gains for the position part and orientation part that are summarized in only one condition by defining parameter $\alpha_i$. By employing the structure of controller (33), the condition is further shortened to

$$\frac{2k_{c_i}(\boldsymbol{\Sigma})k_{e_i}(\boldsymbol{\Sigma})}{k_{c_i}(\boldsymbol{\Sigma}) + k_{e_i}(\boldsymbol{\Sigma})} > \frac{1}{\gamma_1^2} + \left(\frac{1}{\gamma_2^2} + \alpha_i\gamma_2^2\right)L_p + \frac{L_\theta}{\gamma_3^2} \tag{41}$$

for $i = \{p,\, R\}$. Since the left term is minimal for $\underline{k}_{c_i}$, $\underline{k}_{e_i}$, the condition is simplified to (40). ■

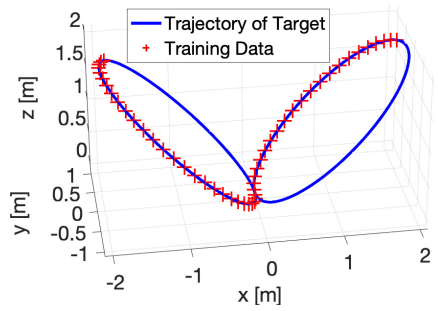


Fig. 4: *"Butterfly"* trajectory of the moving target. The target also rotates around world axis $z$ as given by (45).

As long as the minimum controller gains $k_{c_i}(\boldsymbol{\Sigma})$, $k_{e_i}(\boldsymbol{\Sigma})$ of (33) meet the gain condition (40), stability is assured. The purpose of having uncertainty-adjustable controller gains is to achieve better noise attenuation. Hence, small gains are desired if it does not alter the control performance.

In the next section we will show how to obtain the Lipschitz constants $L_p$ and $L_\theta$ that are used in Theorem 1 and Corollary 1.

### 4.3 Calculation of Lipschitz Constant

This section aims to show a method to calculate the Lipschitz constants of the *GP*-mean function $\boldsymbol{\mu}\big(\breve{\mathbf{g}}_{wo}\big)$ that are necessary for designing the controller gains (33).

By discretizing $\mathcal{X}$ properly one can estimate

$$L_i = \sup_{\boldsymbol{x}\in\mathcal{X}} \left\| \frac{\partial \boldsymbol{\mu}_i(\boldsymbol{x})}{\partial \boldsymbol{x}} \right\|, \quad i \in \{1, \ldots, 6\}. \tag{42}$$

Here, we use the notation $\boldsymbol{x} = [\boldsymbol{x}_1^\intercal\ \boldsymbol{x}_2^\intercal]$, $\boldsymbol{x}_1,\ \boldsymbol{x}_2 \in \mathbb{R}^3$. Then, the Lipschitz constants $L_p,\ L_\theta$ are calculated from $\left\|\frac{\partial \boldsymbol{\mu}}{\partial \boldsymbol{x}_1}\right\| \leq \sqrt{L_1^2 + L_2^2 + L_3^2} = L_\theta$, $\left\|\frac{\partial \boldsymbol{\mu}}{\partial \boldsymbol{x}_2}\right\| \leq \sqrt{L_4^2 + L_5^2 + L_6^2} = L_p$. For notational simplicity, restate (9) with $\mathbf{k}_{\boldsymbol{\varphi}_i}^\intercal(\boldsymbol{x}) \coloneqq \mathbf{k}_{\boldsymbol{\varphi}_i}^\intercal(\boldsymbol{x}, \boldsymbol{X})$ and $\boldsymbol{\tau}_i \coloneqq \left(\mathbf{K}_{\boldsymbol{\varphi}_i} + \sigma_{n,i}^2 \boldsymbol{I}M\right)^{-1} \boldsymbol{Y}_i$ as $\boldsymbol{\mu}_i(\boldsymbol{x}) = \sum_{m=1}^{M} \mathbf{k}_{\boldsymbol{\varphi}_i,m}(\boldsymbol{x})\boldsymbol{\tau}_{i,m}$. Then, computing the derivative of the *SE-ARD kernel* (10) as

$$\frac{\partial \mathbf{k}_{\boldsymbol{\varphi}_i,m}(\boldsymbol{x})}{\partial \boldsymbol{x}_j} = \mathbf{k}_{\boldsymbol{\varphi}_i,m}(\boldsymbol{x}) \frac{\boldsymbol{x}_j^{\{m\}} - \boldsymbol{x}_j}{l_{i,j}^2}, \quad j \in \{1, \ldots, 6\}, \tag{43}$$

then the norm in (42) obeys

$$\left\| \frac{\partial \boldsymbol{\mu}_i(\boldsymbol{x})}{\partial \boldsymbol{x}} \right\| = \sqrt{\sum_{j=1}^{6} \left( \sum_{m=1}^{M} \boldsymbol{\tau}_{i,m} \mathbf{k}_{\boldsymbol{\varphi}_i,m}(\boldsymbol{x}) \frac{\boldsymbol{x}_j^{\{m\}} - \boldsymbol{x}_j}{l_{i,j}^2} \right)^2}. \tag{44}$$

By finding the maximum value in (44) on the discretized $\mathcal{X}$, the Lipschitz constants $L_p,\ L_\theta$ are obtained.

## 5. Simulation Experiment

This section aims to show the effectiveness of the proposed control scheme (33) in two simulations. The first simulation showcases the effectiveness of using pose information $\breve{\mathbf{g}}_{wo}$ rather than only the position $\boldsymbol{p}_{wo}$ from the author's previous work [15]. In the second simulation we show the advantage of using variance-dependent varying gains when the visual measurements (6) are corrupted by noise. Feature extractions from visual measurements always cause noise. We consider the combination of two kinds of noise: a stochastic signal and an impulsive signal.

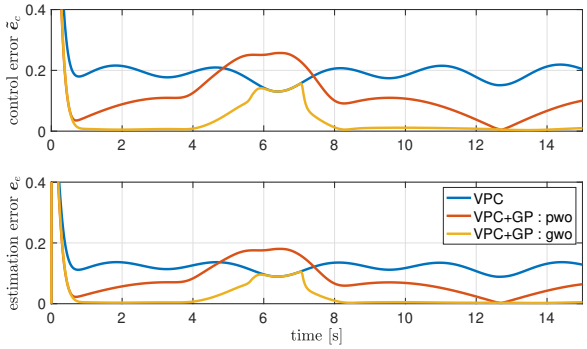


Fig. 5: Estimation and control error.

Table 1: Root Mean Square Error of total error $[\tilde{\boldsymbol{e}}_c^\intercal\ \boldsymbol{e}_e^\intercal]^\intercal$

| | no GP | $\boldsymbol{\mu}(\bar{\boldsymbol{p}}_{wo})$ | $\boldsymbol{\mu}\big(\breve{\mathbf{g}}_{wo}\big)$ |
|---|---|---|---|
| RMSE | 0.275 | 0.223 | **0.167** |

Now, define the following specific simulation environment. The target moves according to the body velocity

$$\begin{aligned} \boldsymbol{v}_{wo}^b &= [\pm \sin(t)\ \cos(t)\ \sin(t)]^\intercal \\ \boldsymbol{\omega}_{wo}^b &= [0\ \ 0\ \ (\pi/2)\sin(0.5t)]^\intercal, \end{aligned} \tag{45}$$

starting from $t = 0$ and the initial position $\boldsymbol{p}_{wo}(0) = [0,\ 0,\ 0]^\intercal$ and orientation $\boldsymbol{\xi\theta}_{wo}(0) = [0,\ 0,\ 0]^\intercal$, resulting in a butterfly-like trajectory (Fig. 4), and continuing to move on the right wing in a region of observed data first. Even though the body velocity (45) is not described by a function of $\breve{\mathbf{g}}_{wo}$, it is still possible to learn $\boldsymbol{V}_{wo}^b\big(\breve{\mathbf{g}}_{wo}\big)$ because of its periodic motion. Note that, depending on the wing, the target approaches the origin at two different orientations $\boldsymbol{\theta}_{wo} = 0$ and $\boldsymbol{\theta}_{wo} = \pi$. It is assumed that only half of each wing can be measured, resulting in a total of $M = 50$ data-pairs indicated by red crosses in Fig. 4. The method of obtaining the data and training a *GP* model follows the discussion in Section 3.2, where the *GP* model is trained on the *VMO* estimate by accurate enough $\breve{\mathbf{g}}_{wo} \approx \breve{\mathbf{g}}_{wo}$ with high estimation gain $k_e^{\text{train}}$. The total simulation time is 15s. Also define the control error $\tilde{\boldsymbol{e}}_c \coloneqq vec\big(\boldsymbol{g}_d^{-1}\boldsymbol{g}_{co}\big)$ when using the real target's pose instead of the estimate $\bar{\boldsymbol{g}}_{co}$ to showcase the influence of noise on the pursuit problem.

### 5.1 Performance Comparison with Static Gains

To prove the benefit of using pose information $\breve{\mathbf{g}}_{wo}$ for the *GP* model, in this simulation it competes against the standard *VPC* in [9] (no GP) and the author's previous work of using the position $\bar{\boldsymbol{p}}_{wo}$ only [15]. The diagonal gain elements are all set as $k_e = 25$, $k_c = 20$. The results are shown in Fig. 5. It is easily observed that using a *GP* model with pose estimate $\breve{\mathbf{g}}_{wo}$ always outperforms $\bar{\boldsymbol{p}}_{wo}$ and the standard *VPC*. When the target moves outside the trained data path (from $t = 4\text{s} \sim 8\text{s}$), $\bar{\boldsymbol{p}}_{wo}$ performs worse than standard *VPC* which results from a misprediction due to crossing the trained data path. It can be inferred that $\bar{\boldsymbol{p}}_{wo}$ imposes a disadvantage at predicting the target motion well even on trained data path if it is rotating, whilst nearly zero state error in both control and estimation is achieved for $\breve{\mathbf{g}}_{wo}$. We achieve a 25% lower *RMSE* when using $\breve{\mathbf{g}}_{wo}$ compared to $\bar{\boldsymbol{p}}_{wo}$ (see Table 1).

### 5.2 Noise Attenuation with Varying Gains

In order to show the advantage of the varying gain, the following simulation incorporates noise in the visual measure-

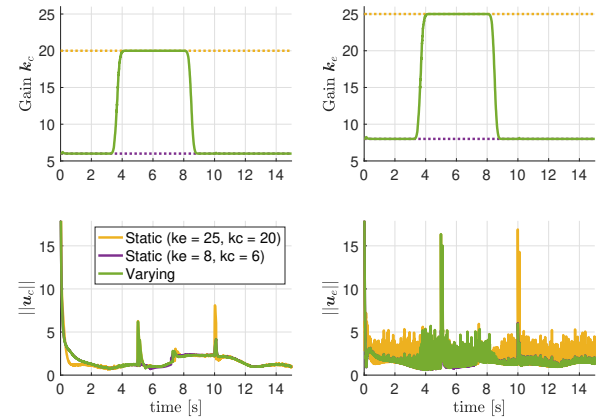


(a)

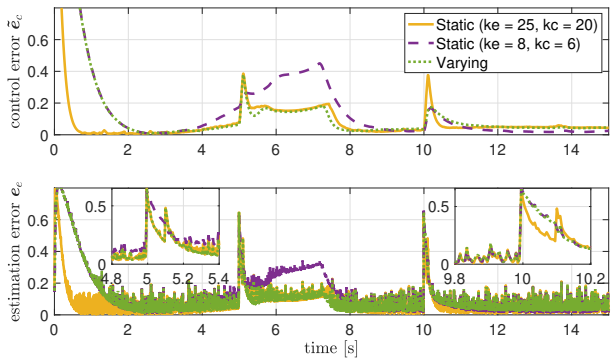


(b)

Fig. 6: (a) control and observer inputs with varying gains, (b) estimation and control error.

ments (6). For *GP* learning phase it is assumed that the measured pose $\check{\boldsymbol{g}}_{wo}$ and target velocity $\boldsymbol{V}_{wo}^{b}$ are both corrupted by Gaussian noise $\mathcal{N}\left(0,\, 0.1^2\right)$. Then, the obtained *GP* model results in estimated Lipschitz constants $L_p = 1.75$ and $L_\theta = 2.53$ by using the result from (44). Finally, by setting the design parameters in Corollary 1 as $\gamma_1 = 4$, $\gamma_2 = 1$, $\gamma_3 = 1$, different from the authors previous work [15] the varying gain function for estimation and control are hereafter chosen as

$$\begin{aligned} k_{c_i}(\boldsymbol{\Sigma}) &= \left(\bar{k}_{c_i} - \underline{k}_{c_i}\right)\left(1 - e^{-1000\boldsymbol{\Sigma}_1^2}\right) + \underline{k}_{c_i}\,, \\ k_{e_i}(\boldsymbol{\Sigma}) &= \left(\bar{k}_{e_i} - \underline{k}_{e_i}\right)\left(1 - e^{-1000\boldsymbol{\Sigma}_1^2}\right) + \underline{k}_{e_i}\,, \end{aligned} \tag{46}$$

with $\bar{k}_{e_i} = 25$, $\underline{k}_{e_i} = 8$, $\bar{k}_{c_i} = 20$, $\underline{k}_{c_i} = 6$, $i = \{p, R\}$. The varying gain function fulfills the designated bounds (33). The reason for choosing (46) rather than the linear function used in [15] is due to the better tuning parameter that allows to adjust to the width of the uncertainty distribution. In the simulation the varying gains compete against both static gains of upper bounds $\bar{k}_{c_i}, \bar{k}_{e_i}$ and lower bounds $\underline{k}_{c_i}, \underline{k}_{e_i}$ , respectively. During control phase, the visual measurement $f$ of the camera model is corrupted by Gaussian noise $\mathcal{N}\left(0,\, 0.0001^2\right)$ and an impulsive noise of power 0.0007 that is added twice on $f_1$ at times $t = 5$s, $t = 10$s and last for 0.1s.

The results are shown in Fig. 6. Since the target moves in the area where the data are available for *GP* training before 4s and after 8s, the varying gain changes between the lower and upper bound values for the same period as seen in the top of Fig. 6a. While the influence of the noise on control input $\boldsymbol{u}_c$ is small for all cases, the observer input $\boldsymbol{u}_e$ becomes noisy. However, noise amplification for the lower gain and varying gain case is smaller than that of the upper gain case. The results of the varying gain and upper gain cases are shown in Fig. 6b, where it can be observed that $\tilde{\boldsymbol{e}}_c$ and $\boldsymbol{e}_e$ are similar after the initial responses converge at around 2s. Furthermore, $\tilde{\boldsymbol{e}}_c$ shows the effect of impulsive noise clearly. The lower gain case shows the best noise attenuation at 5s but the varying gain case has similar performance at 10s since the variance and gains are also small. On the other hand, the upper gain amplifies the impulsive noise at 10s much larger than the other cases. In summary, the varying gain can achieve similar performance as the upper bound static gain but with better noise attenuation.

## 6. Conclusion

This paper proposed a visual pursuit control scheme based on a *GP* model that learns the unknown but pose dependent target body velocity. First, the learning method by using *GP* models was addressed. Second, we proposed a visual pursuit control law in which the learned *GP* mean function is used to cancel the target body velocity, and the variance function to adjust gains. We then derived conditions on the gains to make the estimation and control errors ultimate bounded with high probability. Finally, we demonstrated the effectiveness of the proposed control law in the situation where the visual measurements are corrupted by noise.

## Acknowledgement

This work was supported by JSPS KAKENHI Grant Number 18H01459. This work was partially supported by the European Research Council (ERC) Consolidator Grant "Safe data-driven control for human-centric systems (COMAN)" under grant agreement number 864686.

### References

[1] M. W. Spong, S. Hutchinson, and M. Vidyasagar, *Robot Modeling and Control*, 2nd ed. Wiley, 2020.

[2] K. Hidaka, D. Fujimoto, and K. Sato, "Autonomous Adaptive Flight Control of a UAV for Practical Bridge Inspection Using Multiple-Camera Image Coupling Method," *Journal of Robotics and Mechatronics*, vol. 31, no. 6, pp. 845–854, 2019.

[3] T. Yasui, R. Sugano, K. Sekiguch, and K. Nonaka, "The Push-away Motion of Pest Birds from a Farm Area by a Drone," *Proc. 63rd Japan Joint Automatic Control Conference*, 2E1-3, 2020.

[4] W. Selby, P. Corke, and D. Rus, "Autonomous Aerial Navigation and Tracking of Marine Animals," *Proc. Australian Conference on Robotics and Automation*, pp. 1–7, 2011.

[5] M. Myint, K. Yonemori, K. N. Lwin, A. Yanou, and M. Minami, "Dual-Eyes Vision-Based Docking System for Autonomous Underwater Vehicle: an Approach and Experiments," *Journal of Intelligent & Robotic Systems*, vol. 92, no. 1, pp. 159–186, 2018.

[6] Y. Iwatani and T. Numata, "Indoor Hovering Flight of a Micro Helicopter by Markerless Visual Servo Control Based on Phase Correlation," *SICE Journal of Control, Measurement, and System Integration*, vol. 7, no. 5, pp. 291–296, 2014.

[7] S. A. P. Quintero, D. A. Copp, and J. P. Hespanha, "Robust Coordination of Small UAVs for Vision-Based Target Tracking Using Output-Feedback MPC with MHE," in *Cooperative Control of Multi-Agent Systems: Theory and Applications*, Y. Wang *et al.*, Eds. Wiley, pp. 51–83, 2017.

[8] L. D. Fairfax and P. A. Vela, "A Concurrent Learning Approach to Monocular, Vision-Based Regulation of Leader/Follower Systems," *Proc. 2018 American Control Conference*, pp. 3502–3507, 2018.

[9] T. Hatanaka, N. Chopra, M. Fujita, and M. W. Spong, *Passivity-Based Control and Estimation in Networked Robotics*. Springer, 2015.

[10] C. E. Rasmussen and C. K. I. Williams, *Gaussian Processes for Machine Learning*. MIT Press, 2006.

[11] G. Chowdhary, H. A. Kingravi, J. P. How, and P. A. Vela, "Bayesian Nonparametric Adaptive Control Using Gaussian Processes," *IEEE Transactions on Neural Networks and Learning Systems*, vol. 26, no. 3, pp. 537–550, 2015.

[12] F. Berkenkamp, R. Moriconi, A. P. Schoellig, and A. Krause, "Safe Learning of Regions of Attraction for Uncertain, Nonlinear Systems with Gaussian Processes," *Proc. 55th IEEE Conference on Decision and Control*, pp. 4661–4666, 2016.

[13] T. Beckers, D. Kulić, and S. Hirche, "Stable Gaussian Process Based Tracking Control of Euler–Lagrange Systems," *Automatica*, vol. 103, pp. 390–397, 2019.

[14] Y. Ito, K. Fujimoto, and Y. Tadokoro, "Kernel-Based Hamilton–Jacobi Equations for Data-Driven Optimal and H-Infinity Control," *IEEE Access*, vol. 8, pp. 131 047–131 062, 2020.

[15] J. Yamauchi, T. Beckers, M. Omainska, T. Hatanaka, S. Hirche, and M. Fujita, "Visual Pursuit Control with Target Motion Learning via Gaussian Process," *Proc. 59th SICE Annual Conference*, pp. 1365–1372, 2020.

[16] R. M. Murray, Z. Li, and S. S. Sastry, *A Mathematical Introduction to Robotic Manipulation*. CRC Press, 1994.

[17] N. Wahlström, T. B. Schön, and M. P. Deisenroth, "From Pixels to Torques: Policy Learning with Deep Dynamical Models," *Deep Learning Workshop at the 32nd International Conference on Machine Learning*, 2015.

[18] M. Lang and S. Hirche, "Computationally Efficient Rigid-Body Gaussian Process for Motion Dynamics," *IEEE Robotics and Automation Letters*, vol. 2, no. 3, pp. 1601–1608, 2016.

[19] N. Srinivas, A. Krause, S. M. Kakade, and M. W. Seeger, "Information-Theoretic Regret Bounds for Gaussian Process Optimization in the Bandit Setting," *IEEE Transactions on Information Theory*, vol. 58, no. 5, pp. 3250–3265, 2012.

[20] T. Beckers, J. Umlauft, and S. Hirche, "Mean Square Prediction Error of Misspecified Gaussian Process Models," *Proc. 57th IEEE Conference on Decision and Control*, pp. 1162–1167, 2018.

[21] T. Murao, H. Kawai, and M. Fujita, "Predictive Visual Feedback Control with Eye-in/to-Hand Configuration via Stabilizing Receding Horizon Approach," *IFAC Proceedings Volumes*, vol. 41, no. 2, pp. 5341–5346, 2008.

[22] H. Khalil, *Nonlinear Systems*, 3rd ed. Prentice Hall, 2002.


## Appendix

### A Proof of Lemma 3

By triangle inequality, [22,Lemma 3.1 & 3.2] about Lipschitz continuity in the multivariate case, and the fact that kernel (10) and its partial derivatives are continuous [10], there exist constants $L_p$ and $L_\theta$ on $\mathcal{X}$ such that

$$\begin{aligned}\left\|\boldsymbol{\mu}\left(\breve{\boldsymbol{g}}_{wo}\right)-\boldsymbol{\mu}\left(\breve{\bar{\boldsymbol{g}}}_{wo}\right)\right\| &\leq \left\|\boldsymbol{\mu}(\boldsymbol{p}_{wo},\boldsymbol{\xi\theta}_{wo})-\boldsymbol{\mu}(\bar{\boldsymbol{p}}_{wo},\boldsymbol{\xi\theta}_{wo})\right\| \\ &\quad+\left\|\boldsymbol{\mu}(\bar{\boldsymbol{p}}_{wo},\boldsymbol{\xi\theta}_{wo})-\boldsymbol{\mu}\left(\bar{\boldsymbol{p}}_{wo},\bar{\boldsymbol{\xi}}\bar{\boldsymbol{\theta}}_{wo}\right)\right\| \\ &\leq L_p\left\|\boldsymbol{p}_{wo}-\bar{\boldsymbol{p}}_{wo}\right\|+L_\theta\left\|\boldsymbol{\xi\theta}_{wo}-\bar{\boldsymbol{\xi}}\bar{\boldsymbol{\theta}}_{wo}\right\| \quad (47)\end{aligned}$$

Since $\left\|\boldsymbol{p}_{wo}-\bar{\boldsymbol{p}}_{wo}\right\|=\left\|e^{\hat{\boldsymbol{\xi}}\boldsymbol{\theta}_{wc}}(\boldsymbol{p}_{co}-\bar{\boldsymbol{p}}_{co})\right\|=\left\|\boldsymbol{p}_{ee}\right\|$ and $\boldsymbol{\xi\theta},\ \bar{\boldsymbol{\xi}}\bar{\boldsymbol{\theta}}_{wo}\in B_\pi(0)$, $\left\|\boldsymbol{\xi\theta}_{wo}-\bar{\boldsymbol{\xi}}\bar{\boldsymbol{\theta}}_{wo}\right\|\leq 2\pi$ holds, (34) is obtained from (47). Note that differently to the position, $\boldsymbol{\xi\theta}_{wo}-\bar{\boldsymbol{\xi}}\bar{\boldsymbol{\theta}}_{wo}$ cannot be associated with $\boldsymbol{\xi\theta}_{ee}$. Thus, the worst case bound is employed.

### B Proof of Theorem 1

In this proof, we use the following lemma about the relation between $\boldsymbol{Q}(\boldsymbol{\Sigma})$ and $\tilde{\boldsymbol{Q}}(\boldsymbol{\Sigma})$. The dependency on $\boldsymbol{\Sigma}$ is omitted for simplicity of notation here.

**Lemma 4** Matrix $\tilde{\boldsymbol{Q}}$ is similar to matrix $\boldsymbol{Q}$.

**Proof:** It suffices to find a normal matrix $P$ such that $P\boldsymbol{Q}P^{-1}=\tilde{\boldsymbol{Q}}$. Choose $P=\mathrm{diag}\left(\boldsymbol{I}_6,\ \mathrm{Ad}_{\left(e^{\hat{\boldsymbol{\xi}}\boldsymbol{\theta}_{ce}}\right)}\right)$, then one obtains:

$$P\boldsymbol{Q}P^{-1}=\begin{bmatrix}\boldsymbol{K}_c+\boldsymbol{K}_e & -\boldsymbol{K}_e\mathrm{Ad}_{\left(e^{\hat{\boldsymbol{\xi}}\boldsymbol{\theta}_{ce}}\right)} \\ -\mathrm{Ad}_{\left(e^{-\hat{\boldsymbol{\xi}}\boldsymbol{\theta}_{ce}}\right)}\boldsymbol{K}_e & \mathrm{Ad}_{\left(e^{\hat{\boldsymbol{\xi}}\boldsymbol{\theta}_{ce}}\right)}(\boldsymbol{K}_e-\Gamma)\mathrm{Ad}_{\left(e^{-\hat{\boldsymbol{\xi}}\boldsymbol{\theta}_{ce}}\right)}\end{bmatrix}$$

From the structure of $\boldsymbol{K}_e$ and $\Gamma$, $\mathrm{Ad}_{\left(e^{\hat{\boldsymbol{\xi}}\boldsymbol{\theta}_{ce}}\right)}(\boldsymbol{K}_e-\Gamma)\mathrm{Ad}_{\left(e^{-\hat{\boldsymbol{\xi}}\boldsymbol{\theta}_{ce}}\right)}=\boldsymbol{K}_e-\Gamma$ and $P\boldsymbol{Q}P^{-1}=\tilde{\boldsymbol{Q}}$ holds. Hence, $\tilde{\boldsymbol{Q}}$ is similar to $\boldsymbol{Q}$. ■

We start the proof of Theorem 1 by showing that $S$ is lower and upper bounded by class $\mathcal{K}$ functions $\alpha_1,\ \alpha_2$. Consider the two class $\mathcal{K}$ functions:

$$\alpha_1(\|\boldsymbol{e}\|)=\frac{1}{2}\|\boldsymbol{e}\|^2,\quad \alpha_2(\|\boldsymbol{e}\|)=\|\boldsymbol{e}\|^2. \quad (48)$$

From Proposition 5.3 in [9], $\|\mathrm{sk}(e^{\hat{\boldsymbol{\xi}}\boldsymbol{\theta}})^\vee\|^2\leq\phi(e^{\hat{\boldsymbol{\xi}}\boldsymbol{\theta}})\leq 2\|\mathrm{sk}(e^{\hat{\boldsymbol{\xi}}\boldsymbol{\theta}})^\vee\|^2$ holds when Assumption 2 and 3 are satisfied. Then, $\alpha_1(\|\boldsymbol{e}\|)\leq S\leq\alpha_2(\|\boldsymbol{e}\|)$ holds from (28).

Next, we consider the time derivative of $S$ (28). Applying the proposed input $\boldsymbol{u}$ in (31) to (30) yields

$$\dot{S}=-\boldsymbol{\nu}^\intercal\boldsymbol{K}(\boldsymbol{\Sigma})\boldsymbol{\nu}+\boldsymbol{e}^\intercal\begin{bmatrix}0\\ \mathrm{Ad}_{\left(e^{\hat{\boldsymbol{\xi}}\boldsymbol{\theta}_{ee}}\right)}\end{bmatrix}\left(\boldsymbol{V}^b_{wo}\left(\breve{\boldsymbol{g}}_{wo}\right)-\boldsymbol{\mu}\left(\breve{\bar{\boldsymbol{g}}}_{wo}\right)\right). \quad (49)$$

This is further bounded by *Cauchy-Schwarz-inequality* as

$$\dot{S}\leq-\boldsymbol{\nu}^\intercal\boldsymbol{K}(\boldsymbol{\Sigma})\boldsymbol{\nu}+\|\boldsymbol{e}_e\|\left\|\boldsymbol{V}^b_{wo}\left(\breve{\boldsymbol{g}}_{wo}\right)-\boldsymbol{\mu}\left(\breve{\bar{\boldsymbol{g}}}_{wo}\right)\right\|, \quad (50)$$

where $\left\|\mathrm{Ad}_{\left(e^{\hat{\boldsymbol{\xi}}\boldsymbol{\theta}_{ee}}\right)}\boldsymbol{e}_e\right\|=\|\boldsymbol{e}_e\|$ holds in (50) since a rotation matrix does not change the norm of a vector. From *triangle inequality*, the second term in (50) is bounded as

$$\begin{aligned}&\|\boldsymbol{e}_e\|\left\|\boldsymbol{V}^b_{wo}\left(\breve{\boldsymbol{g}}_{wo}\right)-\boldsymbol{\mu}\left(\breve{\bar{\boldsymbol{g}}}_{wo}\right)\right\|\leq \\ &\|\boldsymbol{e}_e\|\left(\left\|\boldsymbol{V}^b_{wo}\left(\breve{\boldsymbol{g}}_{wo}\right)-\boldsymbol{\mu}\left(\breve{\boldsymbol{g}}_{wo}\right)\right\|+\left\|\boldsymbol{\mu}\left(\breve{\boldsymbol{g}}_{wo}\right)-\boldsymbol{\mu}\left(\breve{\bar{\boldsymbol{g}}}_{wo}\right)\right\|\right). \quad (51)\end{aligned}$$

From *Peter-Paul inequality* and Lemma 3, we have

$$\begin{aligned}&\|\boldsymbol{e}_e\|\left\|\boldsymbol{V}^b_{wo}\left(\breve{\boldsymbol{g}}_{wo}\right)-\boldsymbol{\mu}\left(\breve{\boldsymbol{g}}_{wo}\right)\right\| \\ &\qquad\leq\frac{1}{2\gamma_1^2}\|\boldsymbol{e}_e\|^2+\frac{\gamma_1^2}{2}\left\|\boldsymbol{V}^b_{wo}\left(\breve{\boldsymbol{g}}_{wo}\right)-\boldsymbol{\mu}\left(\breve{\boldsymbol{g}}_{wo}\right)\right\|^2 \quad (52)\\ &\|\boldsymbol{e}_e\|\left\|\boldsymbol{p}_{ee}\right\|\leq\frac{1}{2\gamma_2^2}\|\boldsymbol{e}_e\|^2+\frac{\gamma_2^2}{2}\left\|\boldsymbol{p}_{ee}\right\|^2 \quad (53)\\ &\|\boldsymbol{e}_e\|\cdot 2\pi\leq\frac{1}{2\gamma_3^2}\|\boldsymbol{e}_e\|^2+2\pi^2\gamma_3^2 \quad (54)\end{aligned}$$

with positive constants $\gamma_1,\ \gamma_2,\ \gamma_3>0$. Then, from Lemma 3 and inserting (51) to (54) into (50) yields

$$\begin{aligned}\dot{S}&\leq-\boldsymbol{\nu}^\intercal\boldsymbol{K}(\boldsymbol{\Sigma})\boldsymbol{\nu}+\frac{1}{2}\|\boldsymbol{e}_e\|^2\left(\frac{1}{\gamma_1^2}+\frac{L_p}{\gamma_2^2}+\frac{L_\theta}{\gamma_3^2}\right)\\ &+\frac{\gamma_1^2}{2}\left\|\boldsymbol{V}^b_{wo}\left(\breve{\boldsymbol{g}}_{wo}\right)-\boldsymbol{\mu}\left(\breve{\boldsymbol{g}}_{wo}\right)\right\|^2+\frac{\gamma_2^2L_p}{2}\left\|\boldsymbol{p}_{ee}\right\|^2+2\gamma_3^2\pi^2L_\theta \quad (55)\end{aligned}$$

and by refactoring the terms with $\Gamma$ from (36), we obtain

$$\dot{S} \leq -\boldsymbol{e}^\top \tilde{\boldsymbol{Q}}(\boldsymbol{\Sigma})\boldsymbol{e} + \frac{\gamma_1^2}{2}\left\| \boldsymbol{V}_{wo}^b\left(\check{\boldsymbol{g}}_{wo}\right) - \boldsymbol{\mu}\left(\check{\boldsymbol{g}}_{wo}\right)\right\|^2 + 2\gamma_3^2\pi^2 L_\theta$$

$$\tilde{\boldsymbol{Q}}(\boldsymbol{\Sigma}) \coloneqq \begin{bmatrix} \boldsymbol{K}_c(\boldsymbol{\Sigma}) + \boldsymbol{K}_e(\boldsymbol{\Sigma}) & -\boldsymbol{K}_e(\boldsymbol{\Sigma})\mathrm{Ad}_{\left(e^{\hat{\xi}\theta_{ce}}\right)} \\ -\mathrm{Ad}_{\left(e^{-\hat{\xi}\theta_{ce}}\right)}\boldsymbol{K}_e(\boldsymbol{\Sigma}) & \boldsymbol{K}_e(\boldsymbol{\Sigma}) - \Gamma \end{bmatrix}.$$

From Lemma 4, $\tilde{\boldsymbol{Q}}(\boldsymbol{\Sigma})$ is positive definite when $\boldsymbol{Q}(\boldsymbol{\Sigma})$ is positive definite. Therefore, $\min_{\boldsymbol{\Sigma}} \lambda_{\min}(\tilde{\boldsymbol{Q}}(\boldsymbol{\Sigma})) = \lambda_{\boldsymbol{Q}}$ also holds. From (15) in Lemma 1 and (17), the following holds with probability $\delta \in (0, 1)$:

$$\dot{S} \leq -\lambda_Q \|\boldsymbol{e}\|^2 + \frac{\gamma_1^2}{2}\bar{\Delta}^2 + 2\gamma_3^2\pi^2 L_\theta\,. \tag{56}$$

Thus, using a positive constant $\eta \in (0,\ 1)$ yields

$$\dot{S} \leq -\lambda_Q(1-\eta)\|\boldsymbol{e}\|^2 - \lambda_Q\eta\|\boldsymbol{e}\|^2 + \frac{\gamma_1^2}{2}\bar{\Delta}^2 + 2\gamma_3^2\pi^2 L_\theta. \tag{57}$$

Define

$$\zeta(\delta) \coloneqq \sqrt{\frac{\gamma_1^2\bar{\Delta}^2(\delta) + 4\gamma_3^2\pi^2 L_\theta}{2\eta\lambda_Q}} \tag{58}$$

$$\bar{D}_e \coloneqq \{\boldsymbol{e} \in \mathbb{R}^{12} \mid |\boldsymbol{\theta}_{ee}| \leq \pi/2,\ |\boldsymbol{\theta}_{ce}| \leq \pi/2,\ \|\boldsymbol{e}\| \geq \zeta\}, \tag{59}$$

then the following holds with probability $\delta$:

$$\mathcal{P}\left\{\ \dot{S} < 0,\ \forall \boldsymbol{e} \in \bar{D}_e\ \right\} \geq \delta \tag{60}$$

Thus, from [22] it follows that the error $\boldsymbol{e}$ is ultimately bounded with probability, and the ultimate bound is derived as

$$\alpha^{-1}(\alpha_2(\zeta_(\delta))) = \sqrt{2}\zeta(\delta) = \sqrt{\frac{\gamma_1^2\bar{\Delta}^2(\delta) + 4\gamma_3^2\pi^2 L_\theta}{\eta\lambda_Q}}. \tag{61}$$

This completes the proof.


**Marco Omainska**

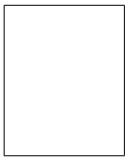

received the B.Sc. and M.Sc. degree in cybernetics from the University of Stuttgart, Germany, in 2016 and 2019, respectively. He is currently working towards his Ph.D. degree at the Information Physics and Computation Department at The University of Tokyo. His research interests include vision-based estimation and control with machine learning, and cooperative control of human-robotic networks.

**Junya Yamauchi** (Member)

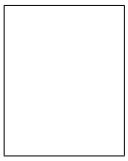

received the Ph.D. degree from Tokyo Institute of Technology in 2018. He was an assistant professor at Tokyo Institute of Technology from 2018 to 2020, and he is currently an assistant professor at The University of Tokyo from 2020. His research interests include vision-based estimation and control, and cooperative control of human–robotic networks.

**Thomas Beckers**

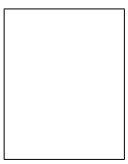

is a postdoctoral researcher at the Department of Electrical and Systems Engineering, University of Pennsylvania. In 2020, he successfully defended his PhD thesis at the Technical University of Munich (TUM), Germany. He received the B.Sc. and M.Sc. degree in electrical engineering in 2010 and 2013, respectively, from the Technical University of Braunschweig, Germany. In 2018, he was a visiting researcher at the University of California, Berkeley. His research interests include data-driven based identification and control, nonparametric systems, and formal methods for safe learning.

**Takeshi Hatanaka** (Member)

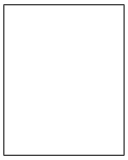

received the Ph.D. degree in applied mathematics and physics from Kyoto University in 2007. He then held faculty positions at Tokyo Institute of Technology and Osaka University. Since April 2020, he is an associate professor at Tokyo Institute of Technology. He is the coauthor of "Passivity-Based Control and Estimation in Networked Robotics" (Springer, 2015), coauthor of "Control of Multi-agent Systems" (Corona Publishing Co., 2015) and the editor of "Economically-enabled Energy Management: Interplay between Control Engineering and Economics" (Springer Nature, 2020). His research interests include cyber-physical & human systems and networked robotics. He received the Kimura Award (2017), Pioneer Award (2014), Outstanding Book Award (2016), Control Division Conference Award (2018), Takeda Prize (2020), and Outstanding Paper Awards (2009, 2015, 2020) all from The Society of Instrumental and Control Engineers (SICE). He also received 3rd IFAC CPHS Best Research Paper Award (2020) and 10th Asian Control Conference Best Paper Prize Award (2015). He is serving/served as an AE for IEEE TSCT and SICE JCMSI, and is a member of the Conference Editorial Board of IEEE CSS. He is a senior member of IEEE.

**Sandra Hirche**

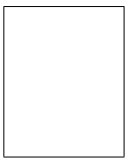

received the Diplom-Ingenieur degree in aeronautical engineering from Technical University Berlin, Germany, in 2002 and the Doktor-Ingenieur degree in electrical engineering from Technical University Munich, Germany, in 2005. From 2005 to 2007 she was awarded a Postdoc scholarship from the Japanese Society for the Promotion of Science at the Fujita Laboratory, Tokyo Institute of Technology, Tokyo, Japan. From 2008 to 2012 she has been an associate professor at Technical University Munich. Since 2013 she is TUM Liesel Beckmann Distinguished Professor and has the Chair of Information-oriented Control in the Department of Electrical and Computer Engineering at Technical University Munich. Her main research interests include cooperative and distributed networked control as well as learning control with applications in human–robot interaction, multi-robot systems, and general robotics. She has published more than 150 papers in international journals, books, and refereed conferences.

**Masayuki Fujita** (Member, Fellow)

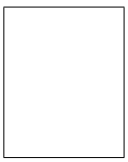

is a Professor and the Course Chair at The University of Tokyo, a Professor Emeritus and a Visiting Professor at Tokyo Institute of Technology. He is also the 2021 president of SICE. He was the Research Supervisor for the Japan Science and Technology Agency Core Research for Evolutional Science and Technology from 2012 to 2020. He received the Eng.D. degree in electrical engineering from Waseda University, Tokyo, in 1987. Prior to his appointment at The University of Tokyo, he held professor/faculty appointments at Tokyo Institute of Technology, Kanazawa University, and the Japan Advanced Institute of Science and Technology. His research interests include passivity-based control in robotics and robust control. He is the coauthor of the book Passivity-Based Control and Estimation in Networked Robotics (Springer, 2015). He was the IEEE Control Systems Society (CSS) Vice President of Conference Activities and a member of the CSS Board of Governors. He served as the General Chair of the 2010 IEEE Multi-Conference on Systems and Control. He was a recipient of the 2008 IEEE Transactions on Control Systems Technology Outstanding Paper Award, a Plenary Lecturer at the 54th IEEE Conference on Decision and Control in 2015, and CSS Distinguished Lecturer from 2017 to 2019. He is a Fellow of the IEEE and SICE.